Journal of Theoretical and Applied Vibration and Acoustics 11 (1) 84-108 (2025)

I S A V

Journal of Theoretical and Applied Vibration and Acoustics

journal homepage: http://tava.isav.ir

PSO-Based reciprocal force generation for structural resonance via stepper motor and accelerometer feedback

Ali Rahmanikhah [a], **Mussa Mahmoudi** [b,*], **Amir Zayeri Baghlani Nejad** [c]

[a] *Ph.D. Student, Civil Engineering Department, Shahid Rajaee Teacher Training University, Tehran, IRAN*

[b] *Full Professor of Structural Engineering, Civil Engineering Department, Shahid Rajaee Teacher Training University, Tehran, IRAN*

[c] *Assistant Professor, Jundi-Shapur University of Technology, Dezful, IRAN*

Research Article

ARTICLE INFO

Article history:
Received 6 October 2024

Received in revised form
28 January 2025

Accepted 07 April 2025

Available online 30 July 2025

Keywords:
Structural resonance

Particle Swarm Optimization (PSO)

Vibration control

Accelerometer (ADXL345)

Structural health monitoring (SHM)

ABSTRACT

This study presents a device designed to induce and optimize structural resonance using a Raspberry Pi, an ADXL345 accelerometer, and a stepper motor controlled by a Particle Swarm Optimization (PSO) algorithm. The device generates vibrations through a reciprocating force applied by the stepper motor to a mass, aiming to resonate with the natural frequencies of the structure. Experimental results demonstrate a significant amplification of acceleration in the X direction as the optimization process progresses, confirming the achievement of structural resonance. The PSO algorithm effectively optimized the motor speed, allowing the system to self-adjust to the structure's dynamic characteristics without requiring detailed prior knowledge of the structure. The results indicate the system's potential for applications in structural health monitoring (SHM), non-destructive testing (NDT), and active vibration control. By providing an adaptable and efficient method for exciting and detecting resonance, this study offers valuable insights into structural dynamics and vibration analysis. Future research will focus on enhancing the device's

* Corresponding author. Tel.: (+98) 912 390 6454

E-mail address: m.mahmoudi@sru.ac.ir (M. Mahmoudi)

http://dx.doi.org/10.22064/tava.2025.2042737.1252

functionality and expanding its application to various structural systems, thereby contributing to the development of safer and more resilient infrastructures.

Nomenclature

SHM	Structural Health Monitoring
PSO	Particle Swarm Optimization
NDT	Non-Destructive Testing
FFT	Fast Fourier Transform
MEMS	Micro- Electro- Mechanical System

1. Introduction

The field of structural health monitoring (SHM) and vibration control has witnessed remarkable advancements in recent years, driven by the integration of cutting-edge sensors, sophisticated control algorithms, and optimization techniques. For instance, Ref. [1] provided an extensive review of wireless sensor networks for SHM, emphasizing the evolution from basic systems to modern sensor boards capable of precise micro-vibration measurements, particularly for bridge monitoring and earthquake damage assessment. Similarly, Ref. [2] highlighted the application of MEMS-based accelerometers in monitoring blast-induced ground vibrations, stressing the significance of sensor attributes such as sensitivity and bandwidth for detecting micro-vibrations. Complementing these works, Ref. [3] introduced a low-cost vibration monitoring system that utilizes a Raspberry Pi and a MEMS accelerometer for real-time monitoring in smart buildings, illustrating the trend towards more portable and accessible SHM solutions.

Control algorithms are equally pivotal in vibration mitigation. Ref. [4] demonstrated the efficacy of Particle Swarm Optimization (PSO) and other algorithms, such as Genetic Algorithm and Differential Evolution, in controlling structural vibrations using piezoelectric sensors and actuators. Expanding on these methods, Ref. [5] discussed adaptive intelligent techniques, including fuzzy logic and neural networks, combined with smart materials such as piezoelectric actuators, to address nonlinearities and uncertainties in structural systems. Resonance analysis and optimization have also been areas of significant focus. Ref. [6] designed a resonant micro-accelerometer optimized via an enhanced differential evolution algorithm, achieving high precision in resonant frequency detection. Ref. [7] compared traditional and simulation-based approaches in torsional vibration analysis, demonstrating improved accuracy in predicting natural frequencies.

In vibration-based SHM, Ref. [8] reviewed dynamic testing and damage detection techniques for bridges, while Ref. [9] traced the evolution of structural control systems from passive to active technologies in civil engineering. Ref. [10] proposed a novel wavelet transform-based approach

for vibration analysis in rotating machinery, enhancing fault detection through improved wavelet techniques. Collectively, these studies highlight the multidisciplinary advancements in SHM and vibration control, emphasizing the role of MEMS sensors, control algorithms, and optimization techniques in enhancing structural safety and performance across diverse applications.

The development of shaking tables has also benefited from advancements in optimization. Ref. [11] introduced a novel harmonic detection method for electrohydraulic servo systems, integrating PSO with simulated annealing (SA) to improve detection accuracy and efficiency. Ref. [12] applied a PSO-based method for estimating acceleration harmonics in hydraulic shaking tables, enabling effective cancellation of parasitic motions caused by nonlinearities. These innovations exemplify the potential of optimization algorithms in addressing complex structural dynamics challenges. Several studies have explored optimal configurations of piezoelectric actuators and sensors for structural vibration control. For example, Ref. [13] reviewed optimization criteria for sensor and actuator placement, while Refs. [14] and [15] investigated placement strategies to minimize control energy and maximize sensor output in functionally graded material beams. Similarly, Ref. [16] examined optimal configurations on cylindrical shells, considering controllability and observability. Other researchers [17] [18], employed genetic and evolutionary algorithms for actuator placement optimization, aiming to maximize control effectiveness and minimize applied voltage. Researchers ([19], [20], and [21]) further explored multi-objective optimization techniques for piezoelectric smart structures, highlighting the advancements in optimizing structural configurations for vibration control.

Despite these advancements, a critical gap remains in developing adaptable, self-optimizing devices capable of inducing and optimizing structural resonance without prior knowledge of the structural characteristics. Addressing this gap, the present study introduces a device that combines a Raspberry Pi, an ADXL345 accelerometer, a stepper motor, and a PSO algorithm to autonomously adjust its operating parameters and resonate with a structure's natural frequencies. Unlike previous studies, which focused predominantly on vibration control or analysis, this work pioneers the concept of a self-tuning system for resonance induction. By demonstrating the capability to achieve resonance with minimal prior data, this research offers significant potential for applications in SHM, non-destructive testing, and active vibration control. The study's innovative approach lays the groundwork for future advancements in autonomous resonance-based monitoring systems, marking a transformative step in the field.

2. Description of the device

The system, designed to induce structural resonance, relies on a combination of compact and powerful components that enable both precise motion control and accurate acceleration measurements. The Raspberry Pi serves as the central processing unit, orchestrating data acquisition from the accelerometer and controlling the movements of the stepper motor. Its versatility enables the efficient implementation of real-time processing and optimization algorithms, such as Particle Swarm Optimization (PSO). The TB6600 driver provides the necessary interface to manage the stepper motor’s operation, ensuring smooth and reliable motion,

even under high current loads. The term 'step interval' refers to the time interval between successive pulses sent to the stepper motor driver, which determines the rotational speed of the motor. The Denki stepper motor, paired with a custom-designed mechanical system, delivers the reciprocating force essential for generating vibrations in the structure. At the same time, the ADXL345 accelerometer captures real-time acceleration data, enabling precise frequency analysis and resonance detection. Together, these components form a robust platform for experimentation and analysis of structural resonance phenomena—the Specification of used devices illustrated in Table 1 and the assembled fragments depicted in Figure 1.

Table 1: Device Specifications

Component	Photo of the device	Specification
Raspberry Pi		Model: Raspberry Pi 3B+ CPU: Quad Core 1.2GHz Broadcom BCM2837 64-bit RAM: 1GB LPDDR2 GPIO: 40-pin header Operating System: Raspbian or other Linux distributions
ADXL345 Accelerometer		Measurement Range: ±2g/±4g/±8g/±16g Sensitivity: 256 LSB/g for ±2g mode Output Data Rate: 0.1 Hz to 3200 Hz Communication: I²C/SPI Supply Voltage: 2.0 V to 3.6 V
TB6600 Stepper Motor Driver	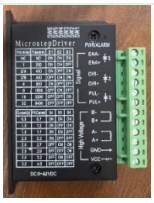	Supply Voltage: 9-42V DC Output Current: 0.5A to 4.5A adjustable Microstep Resolution: 1, 1/2, 1/4, 1/8, 1/16 steps Control Mode: Pulse (PUL), Direction (DIR), Enable (ENA)
Stepper Motor Denki 103H7123-5040		Step Angle: 1.8° Torque: 0.78 N·m (Holding torque) Current/Phase: 3.0A Resistance/Phase: 1.3Ω Inductance/Phase: 2.6 mH

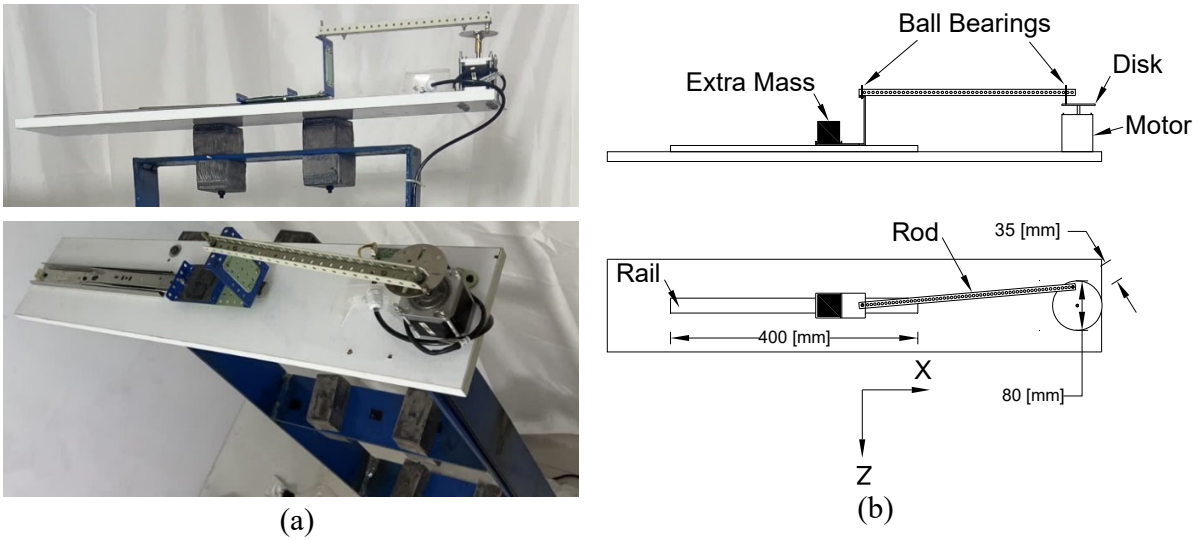

Fig. 1. The reciprocal force generator device, (a): The real device (b): The schematic of the components of the device and dimension.

2.1. Converting rotary motion to reciprocating motion (Acceleration and force)

The acceleration of a reciprocating rod connected to a rotary disc at a point on the disc's perimeter can be derived from the kinematics of circular motion (Figure 2). R represents the radius of the disc and ω the angular velocity of the motor. The position of the ball bearing in the horizontal direction (X-axis) is presented by x(t) in Equation 1. Assuming the rod is constrained to move along the X-axis only, the velocity $V_x(t)$ and acceleration $a_x(t)$ of the rod can be found by differentiating x(t) once and twice respectively as given in Equations (2) and (3). The force for this system is obtained by multiplying the mass by the acceleration, as presented in Equation (4).

$$x(t) = R.Cos(\omega.t) \tag{1}$$

$$V_x(t) = \frac{dx(t)}{dt} = -R.\omega.Sin\ (\omega.t) \tag{2}$$

$$a_x(t) = \frac{dV(t)}{dt} = -R.\omega^2.Cos\ (\omega.t) \tag{3}$$

$$Fx(t) = m.a_x(t) = -m.R.\omega^2.Cos\ (\omega.t) \tag{4}$$

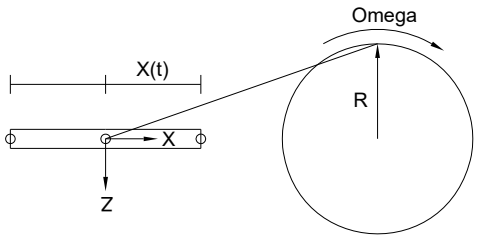

Fig. 2. Converting rotary motion to reciprocating motion

Figure 3 represents the force Fx(t) as a function of time t in a reciprocal motion system. The curve follows a cosine function, illustrating how the force oscillates over time with a negative amplitude. The force varies between positive and negative values, showing periodic behavior typical for harmonic motion.

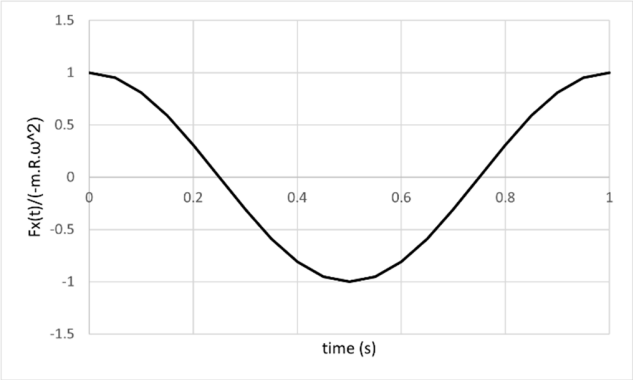

Fig. 3. Force vs Time (Harmonic periodic loading)

2.2. Advantages of stepper motors with micro stepping resolution for lightweight structures

The rotational speed of a stepper motor is directly determined by the pulse frequency provided to its driver. Using the TB6600 driver with the Denki 103H7123-5040 stepper motor, the high micro stepping resolution (1/16 steps) improves smoothness and precision in motion. This makes stepper motors suitable for lightweight systems such as the 3-story experimental frame used in this research. The lightweight structure requires precise, controlled movements, which this motor and driver combination can achieve. Increasing the micro stepping resolution (1/16 steps) reduces mechanical resonance, improves positioning accuracy, and enables smoother motion. These benefits are particularly advantageous for experimental setups that require precise load application or motion control. However, a higher resolution slightly reduces the motor's torque at high speeds, which should be taken into consideration during the design process. Servo motors are often used for high-speed and high-torque applications with feedback control systems, providing superior accuracy in closed-loop operations. However, for lightweight structures, stepper motors with high micro stepping resolution offer a cost-effective and sufficiently precise alternative. Unlike servo motors, stepper motors do not require feedback sensors for operation, simplifying the system design.

The selected stepper motor and TB6600 driver combination are sufficient for the lightweight 3-story experimental frame in this study. The system's bandwidth and resolution are adequate for replicating the small, controlled forces required for the experiments. The system bandwidth for stepper motors depends on the maximum pulse frequency ($f_{pulse,\max}$) that the driver can process without losing steps. For the TB6600 driver, typical bandwidths range from 100 Hz to nearly 6400 Hz, depending on the load and micro stepping. The symbol N_{rps} and N_{rpm} represents the rotational speed of a motor in revolutions per second and minute, respectively, in Equations (5) to (8).

$$N_{rps} = \frac{f_{pulse}}{Microsteps\ per\ revolution} \tag{5}$$

$$Microsteps\ per\ revolution = 200 \times 16 = 3200 \tag{6}$$

$$N_{rpm} = \frac{f_{pulse} \times 60}{3200} = \frac{f_{pulse}}{53.33} \tag{7}$$

For N_{rpm}=120:

$$f_{pulse} = N_{rpm} \times 53.33 = 120 \times 53.33 \approx 6400\ Hz \tag{8}$$

3. PSO algorithm and fitness function

Particle Swarm Optimization (PSO) is an optimization algorithm inspired by the social behavior of birds flocking or fish schooling [22, 23]. Each solution in the search space is represented as a "particle" with a position and velocity. At each iteration, particles update their velocities and positions based on their own best-known position and the best-known position of the swarm. The velocity update equation incorporates three components: inertia, cognitive, and social. The inertia term keeps the particle moving in its current direction. In contrast, the cognitive term pulls the particle toward its best-known position, and the social term pulls it toward the best-known position of the swarm. The velocity update is presented in Equation (9) as follows:

$$v_i(t+1) = w.v_i(t) + c_1.r_1.\left(p_{best,i} - x_i(t)\right) + c_2.r_2.\left(g_{best} - x_i(t)\right) \tag{9}$$

where $v_i(t)$ is the velocity of particle i at iteration t, w is the inertia weight, c1, and c2 are the cognitive and social coefficients, r1 and r2 are random values, $p_{best,i}$ is the particle's best-known position, and g_{best} is the global best-known position. The new position of each particle is then updated as follows:

$$x_i(t+1) = x_i(t) + v_i(t+1) \tag{10}$$

The flowchart given in Figure (4) outlines the process of using the PSO algorithm to optimize the speed parameter in controlling a stepper motor, thereby increasing the Fast Fourier Transform (FFT) magnitude at a target frequency measured by the ADXL345 accelerometer. The system begins by initializing the hardware, including setting up the Raspberry Pi, the ADXL345 accelerometer, and the stepper motor, which is controlled by the TB6600 driver. The ADXL345 accelerometer continuously collects real-time acceleration data from the structure or system to which the device is attached. The Raspberry Pi reads this acceleration data from the accelerometer in the x, y, and z directions. In the next step, the system applies FFT to the accelerometer data, specifically focusing on the x-axis acceleration to analyze the frequency content of the signal. The FFT reveals the dominant frequencies and their respective magnitudes. This frequency analysis is critical for identifying the natural frequencies of the structure or the system on which the device is mounted. To detect the dominant frequencies, the harmonic loading is assigned to the structure, as discussed in section 0. One of these dominant frequencies is selected as the target frequency for

resonance, and the goal of the PSO algorithm is to maximize the magnitude of the FFT at this specific frequency by optimizing the motor speed, which controls the reciprocating motion of the attached mass.

The PSO algorithm is initialized with a swarm of particles, each representing a candidate solution for the motor step interval within a specified range. The particles explore the search space, adjusting the motor speed, which influences the stepper motor's motion and, consequently, the forces generated by the reciprocating mass. The fitness function given in Equation (11) in the PSO algorithm is defined as the magnitude of the FFT at the target frequency f_{target}. During each iteration, the motor speed, xi, is adjusted by the PSO algorithm to optimize this fitness value. The system measures the resulting acceleration signal, a(t), and applies an FFT to determine the magnitude at f_{target}. This magnitude serves as the fitness of each particle. Based on these fitness values, particles update their positions (motor step interval), guided by their own best-known values and the global best. Over successive iterations, the algorithm converges on the motor speed that maximizes the FFT magnitude at f_{target}, achieving resonance. This iterative process continues until the optimal motor speed is identified.

$$fitness(x_i) = \left|FFT(a(t),\, f_{target})\right| \tag{11}$$

At the end of the process, the system achieves an optimized speed for the stepper motor, causing the mass to move in such a way that it generates reciprocal forces matching the natural frequency of the structure. This results in amplified vibrations at the target frequency, as measured by the accelerometer, which is critical for applications such as structural health monitoring or testing the dynamic behavior of structures. Throughout the process, two CSV files are generated: one containing raw acceleration data in the x, y, and z directions along with timestamps and another that logs the FFT frequencies, their magnitudes, and the iteration number during each PSO step. These files provide a detailed record of the experiment, allowing for further analysis of the device's performance. The flowchart in Figure (4) clearly demonstrates how the components of the system work together: the Raspberry Pi acts as the central controller, gathering data from the ADXL345, processing it using FFT, and then using PSO to control the stepper motor’s speed. The result is a system that dynamically adjusts itself to resonate at the desired frequency, highlighting the efficiency of using PSO in this type of real-world optimization problem.

The finishing criteria for the optimization process are defined as follows: the algorithm terminates after a minimum of 10 iterations or when the magnitude of the FFT of the target frequency exceeds twice the magnitude of the second-highest frequency component detected in the structure's vibration. This criterion is selected to ensure the identification of the target mode shape while minimizing the risk of structural damage. It is acknowledged that this criterion may cause the optimization process to stop before the fitness function achieves full convergence. However, the primary objective of the process—revealing the target mode shape and amplifying the target frequency—takes precedence over achieving complete algorithmic convergence. Amplifying the magnitude of the target frequency significantly increases the structure's deflection under resonance, which could potentially lead to damage in critical elements. The 10-iteration threshold

ensures that the vibration duration remains short (approximately 4 seconds), allowing structural damping to rapidly attenuate the response. As a result, the structure remains undamaged under the applied conditions.

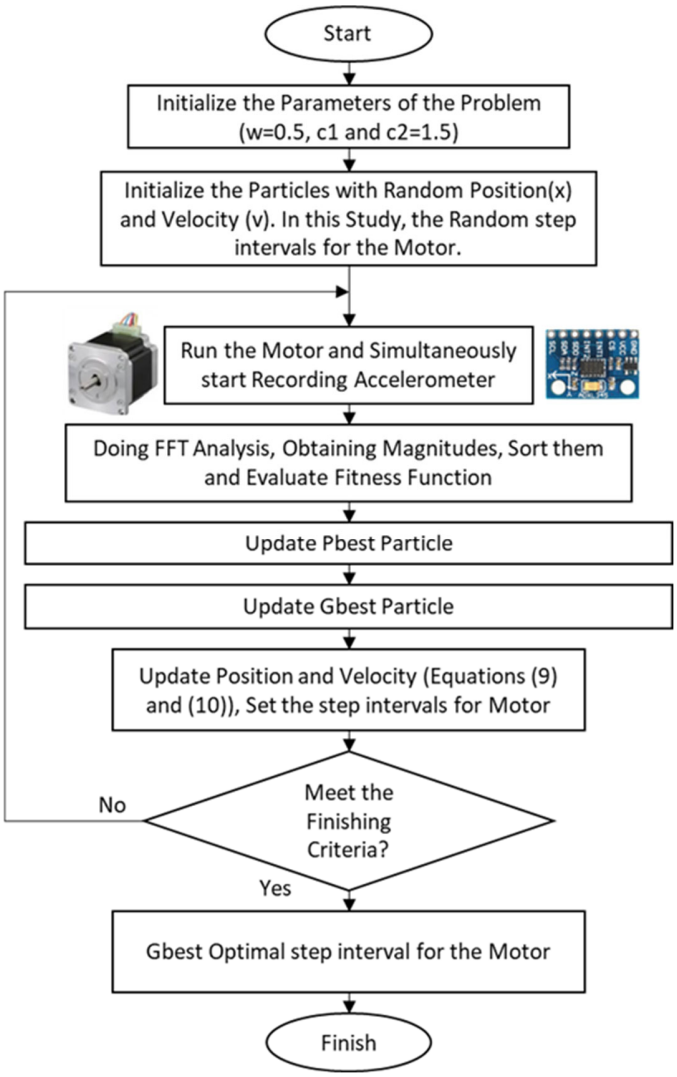

Fig. 4. The PSO flowchart of the device process

In classical methods, forced vibration testing is typically conducted within a frequency range known to excite the structure's dominant dynamic characteristics. For instance, Ref. [24] employed a sine sweep force, ranging from 1Hz to 8Hz and then from 8Hz to 15Hz, to excite a multi-story

timber building. This approach involves manually adjusting the frequency range of the sine force. In contrast, the proposed method in this study focuses on a specific target frequency. It automatically adjusts the excitation vibration frequency using an algorithm, offering a more targeted and efficient approach to resonance induction.

4. Comparison with classical methods

Dynamic testing is essential for determining the dynamic characteristics of civil engineering structures. However, commonly employed devices face significant limitations, including low-frequency resolution in spectral estimates, which hampers the accurate determination of modal damping factors and insufficient energy to excite critical vibration modes [25]. To overcome these issues, specialized devices have been developed in laboratories.

Figure 5.a illustrates a device that excites a structure through the impact of a falling weight on a damper, generating higher acceleration than ambient vibrations [26]. Figure 5.b shows an electrodynamic shaker capable of producing varied input signals, controlled in frequency and amplitude, using a signal generator and power amplifier [25]. For large-scale structures, heavy excitation equipment is required. Figure5.c depicts an eccentric mass vibrator, historically used for testing dams. Although effective in applying sinusoidal forces, it is limited by low force amplitudes at low frequencies and difficulties in force measurement and restraint [25]. Servo-hydraulic shakers, shown in Figure 5d, 5e, and 5f, provide a more effective solution for broad-band excitation within the relevant frequency ranges. Electrodynamic shakers have also been employed for testing multi-story structures. Figure 5g demonstrates a shaker mounted on a four-story structure's roof (Figure 5h) for swept-sine excitation, while Figure 5i depicts two synchronized shakers testing a 13-story reinforced concrete building to determine dynamic characteristics [27]. Figure 5j highlights forced vibration testing on the Sean O'Casey Bridge using paired shakers to generate frequency response functions for modal analysis [25]. Additionally, Figure 5k shows a shaker installed on a six-story steel structure to resonate its main frequencies, applying sinusoidal force vibrations from 0.5 Hz to 10 Hz. Figure 5l presents a method utilizing photogrammetry for extracting structural properties through image processing of filmed markers [28]. Despite advancements, none of these devices automatically adjust forced vibration frequencies to achieve target frequencies. This study introduces a device that integrates an accelerometer and a PSO algorithm to dynamically identify and excite the main frequencies of a structure.

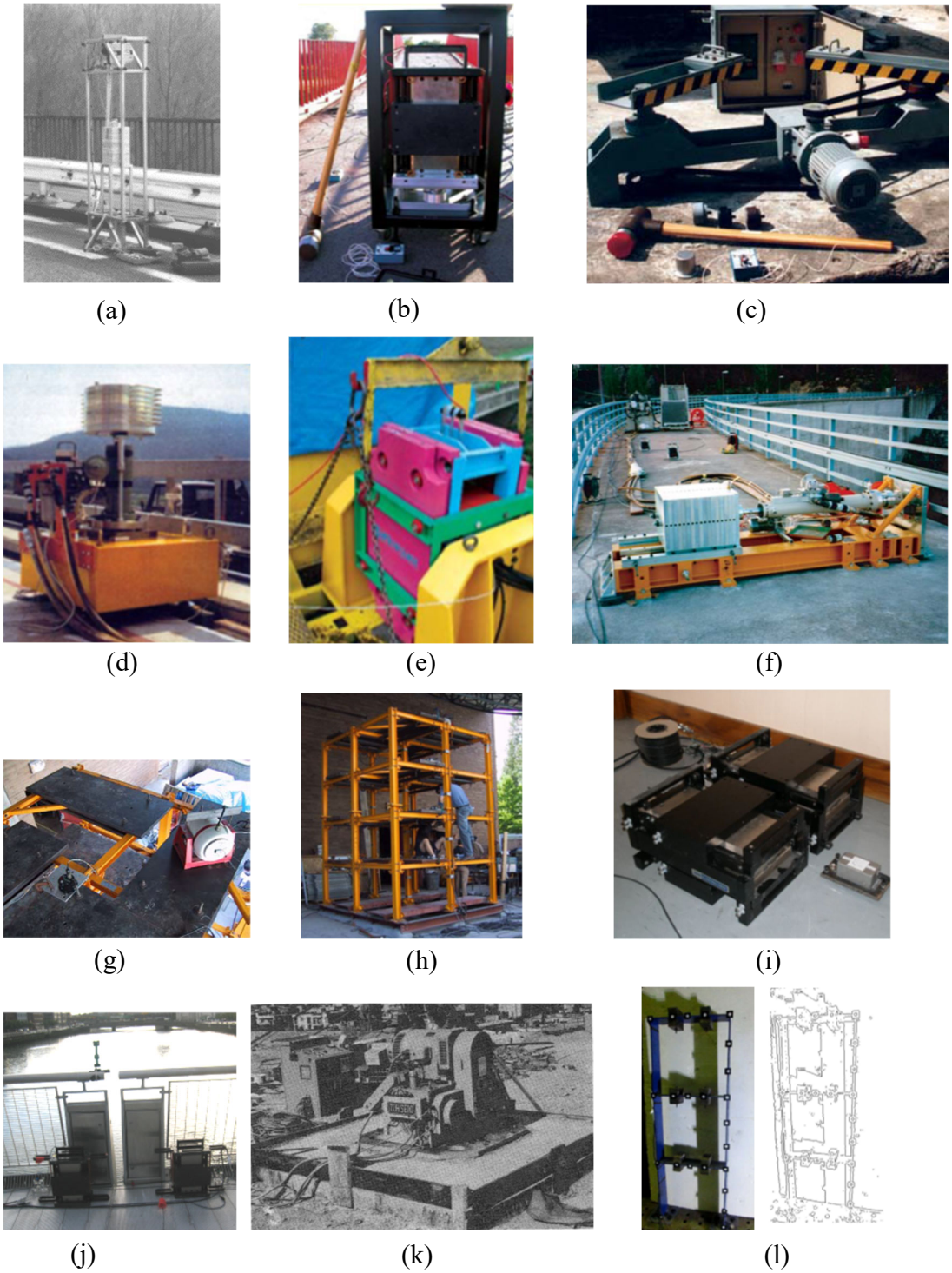

Fig. 5. Dynamic Testing Devices for Civil Engineering Structures (a) A falling weight shaker, (b) an electrodynamic shaker, (c) an eccentric mass vibrator, (d, e, f) servo-hydraulic shakers, (g, h) a motor used as a shaker for testing multi-story structures, (i) two synchronized shakers, (j) paired shakers, (k) a 3-axial eccentric mass shaker, (l) the photogrammetry method for extracting structural properties.

5. Experimental setup

In this case study, a two-dimensional, three-story steel frame was selected for analysis. The frame has a height of 1500 mm and a width of 500 mm, with each story measuring 500 mm in height. In each story, two concentrated masses of 5 kg are attached to the beam, spaced 200 mm apart. The columns at the base are fixed to the foundation. The material properties of the frame include a Young's modulus of 2.1×1010 kg/m2, a density of 7850 kg/m3, and a Poisson's ratio of 0.3. The columns and beams are constructed from steel plates with a width of 110 mm and a thickness of 8 mm, as depicted in Sections a-a and b-b in Figure 6.a. The accelerometer records X-direction accelerations, as defined by the coordinate system in Figure 6.a, at a sampling rate of 240 Hz. Considering the Nyquist frequency, detected frequencies up to 240/2=120 Hz are possible. The structure examined in this study is the same as that analyzed in previous research (Figure 6.b), which employed close-range photogrammetry to extract structural dynamic properties and investigated the capability of proper orthogonal modes in identifying natural frequencies and damping ratios of linear structural systems [29]. However, in this study, three damages were assigned. At points B, C, and F, the beam-to-column connection welds were partially removed (approximately 15 mm on both sides of the beam), as illustrated in Figure 6.c. The additional weight illustrated in Figure 1 was not utilized in the experiment. The combined weight of the rod, rail, and components is approximately 350 grams. The results indicate that this mass is sufficient for the tested structure.

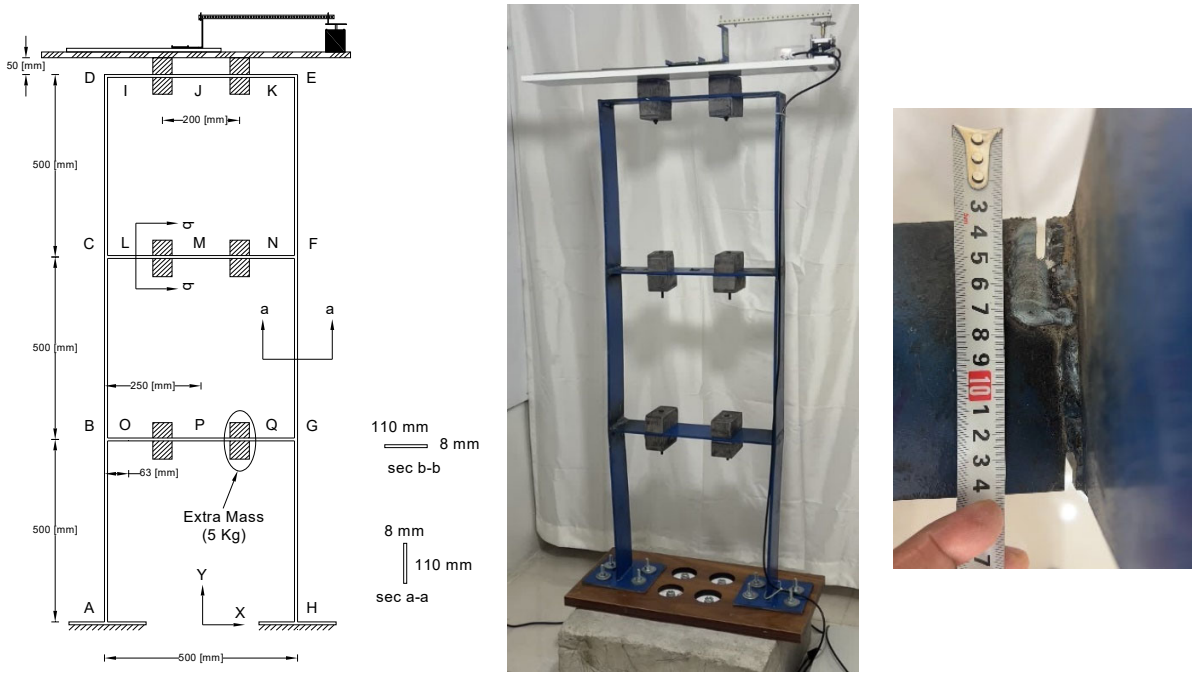

(a) (b) (c)

Fig. 6. The Two-Dimensional, Three-Story Steel Frame, (a): Schematic Drawing (b): Real Structure (c): Assigned Damages at points B, C, and F

This study aims to optimize the stepper motor speed to enhance resonance at the first vibration frequency of the structure. The PSO algorithm was employed to fine-tune the speed parameter, which governs the speed and timing of the motor's reciprocating motion. This speed directly influences the dynamic forces generated by the motor and, consequently, the vibration characteristics measured by the accelerometer. The step interval parameter was varied within a discrete range from 0.01 seconds to 0.0001 seconds. The motor operated at a fixed speed for 4 seconds for each particle, during which the number of harmonic load cycles affecting the structure could vary, as described by Equation (4). The optimization process identified the step interval value that generated a force resonating the structure at its first vibration frequency. However, the methodology can similarly target higher vibration modes, such as the second or third frequencies. During each PSO iteration, the algorithm evaluated the fitness function, defined as the magnitude of FFT of the acceleration signal at the first vibration frequency given in Equation (11). This approach ensured that the optimization was focused on maximizing resonance at the target frequency.

The performance of the proposed device was evaluated through four independent experimental tests. In each test, the accelerometer sensor was positioned at different locations (points P, L, M, and J), and the optimization algorithm was executed independently at each location. During each iteration, the algorithm's best-performing result was recorded as the best particle. The acceleration data corresponding to these best-performing iterations were saved and plotted to demonstrate the algorithm's performance with the fitness function over successive iterations. Additionally, the magnitude of the FFT for each acceleration signal was plotted to illustrate the frequency response. The trends of the fitness function versus iteration and motor step interval versus iteration are presented in subsections 4.1 to 4.4.

5.1. Sensor placement at point P

The sensor is installed at a height of 500 mm on the beam of the first story of the structure, designated as point P in Figure 6a and depicted in Figure 7. The vibration-inducing device is positioned on the roof of the structure, 50 mm above the beam. This device generates vibrations that propagate through the columns and beams from the upper to the lower elevations. Accelerations corresponding to the best particle at each iteration of the algorithm are recorded and presented in Figure 8.a. During the initial iterations 1 to 10, the magnitude of the frequency of the target mode, as observed in the FFT plot in Figure 8.b, becomes increasingly distinct. As the number of iterations increases, the magnitudes of undesired frequencies decrease significantly while the magnitude of the target frequency grows substantially. By the tenth iteration, only the magnitude of the first (target) frequency remains prominent. Figure 8.c illustrates the variation of the best step interval of the motor across iterations. As the number of iterations increases, the motor step interval converges toward the target value. Additionally, the fitness function values improve with each iteration, demonstrating the algorithm's effectiveness (Figure 8.d). The optimization trend indicates the potential for further refinement; however, the termination criteria halt the algorithm once the objective is achieved. It is important to note that excessive iterations could

induce resonance in the structure, potentially leading to damage in certain elements. To mitigate this risk, the maximum number of iterations is limited to 10, ensuring structural integrity while achieving the desired optimization.

Fig. 7. Sensor placement at point P, center of the first-story beam

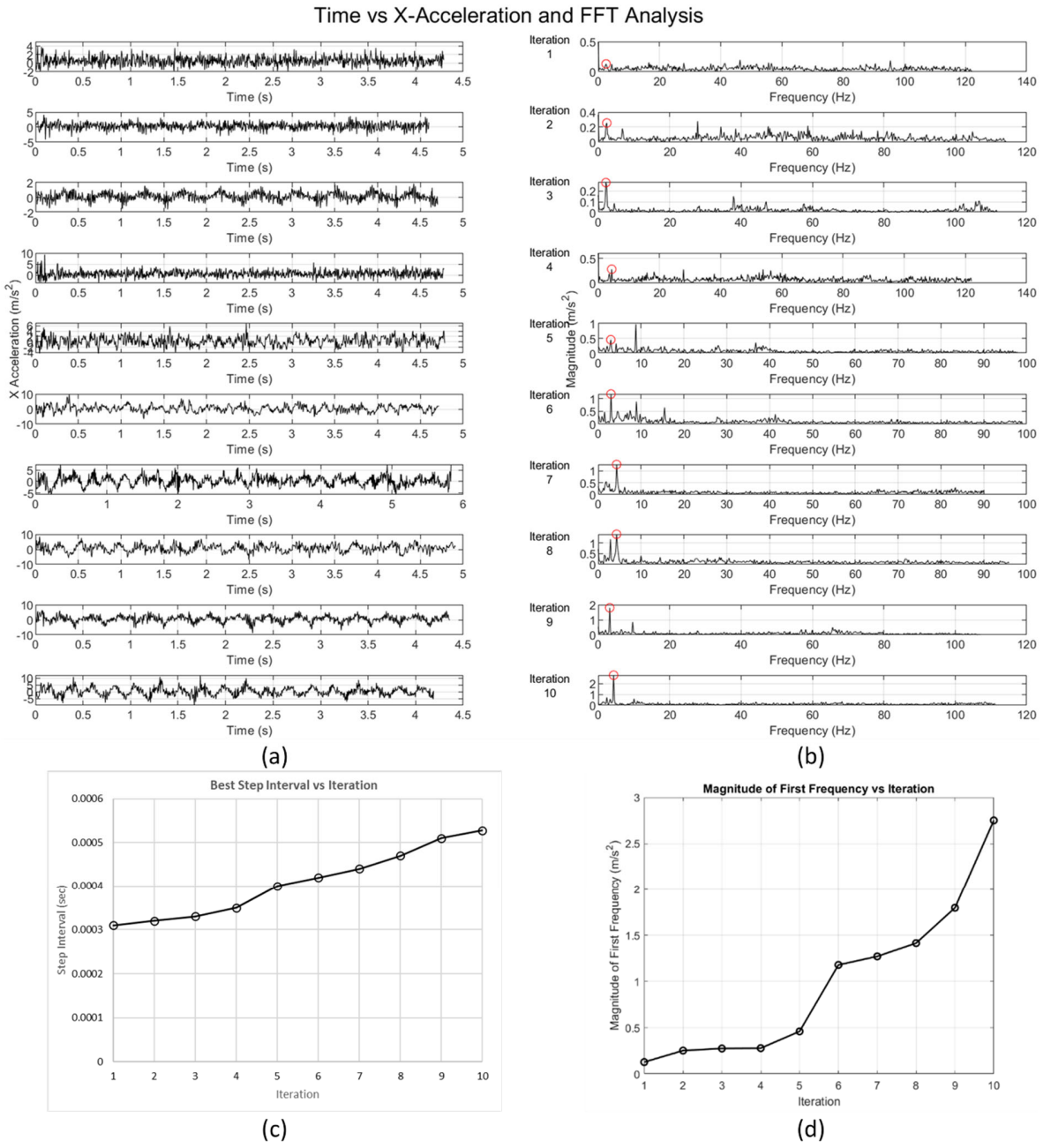

Fig. 8. Algorithm results at point P – (a) X-axis acceleration for best particle per iteration, (b) Acceleration FFT, (c) Best motor step interval vs. iteration, (d) Fitness values vs. iteration

5.2. Sensor placement at point L

The sensor is installed at 1000 mm on the corner of the beam of the second story (Point L, Figure 6.a and 6). Accelerations for the best particle at each iteration are depicted in Figure 10.a. During iterations 1–10, the target frequency's magnitude, as shown in the FFT plot in Figure 10.b, becomes dominant as undesired frequencies diminish. By the tenth iteration, only the target frequency remains prominent. The motor step interval converges toward the target value with increasing iterations (Figure 10.c), and the fitness function improves, confirming the algorithm's effectiveness (Figure 10.d). Optimization halts once the objective is met to prevent excessive iterations, which could induce resonance and structural damage.

Fig. 9. Sensor placement at point L, corner of the second-story beam

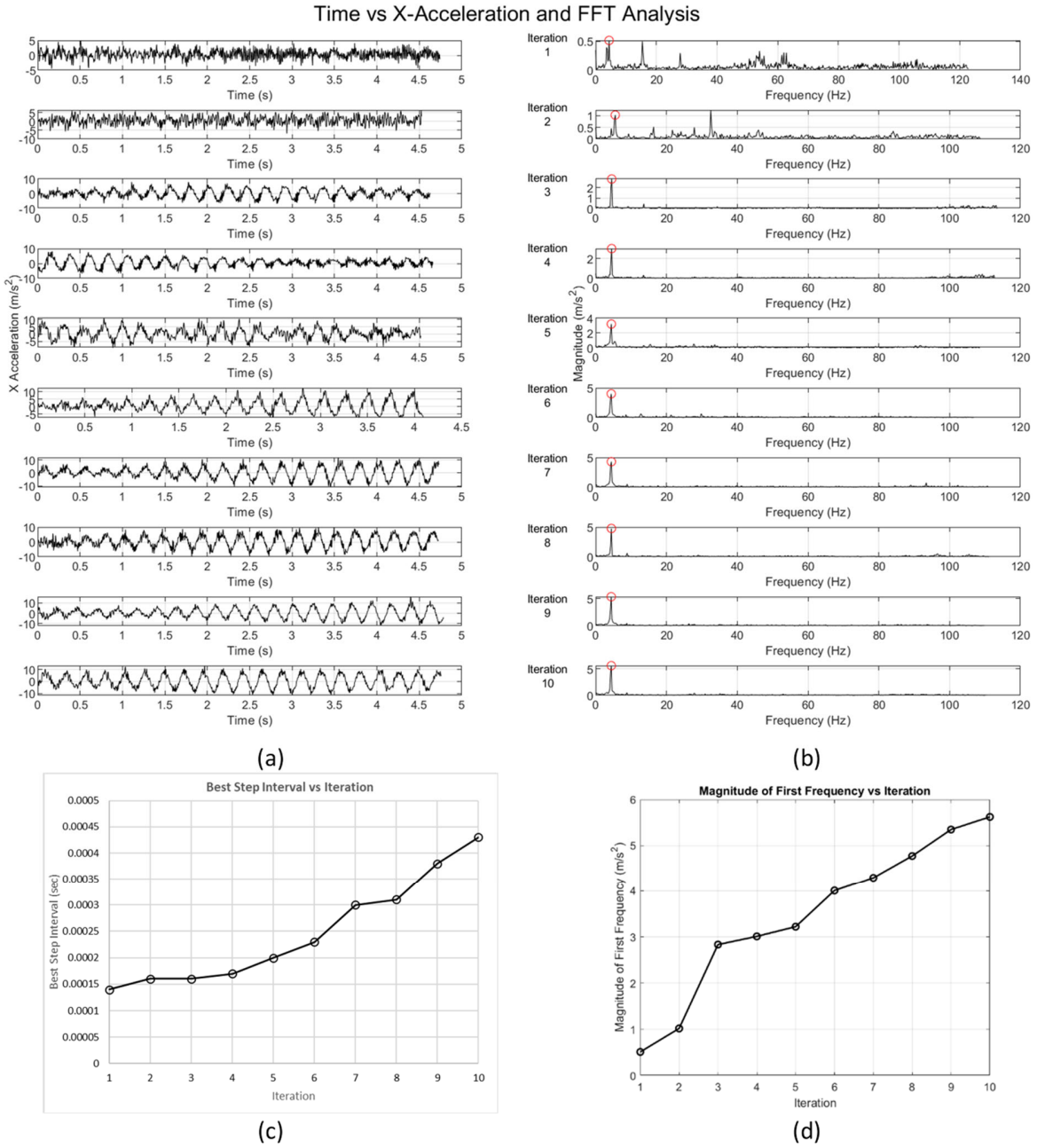

Fig. 10. Algorithm results at point L – (a) X-axis acceleration for best particle per iteration, (b) Acceleration FFT, (c) best motor step interval vs. iteration, (d) Fitness values vs. iteration

5.3. Sensor placement at point M

The sensor is installed at 1500 mm on the center of the third-story beam (Point J, Figures 5a and 12). Recorded accelerations for the best particle across iterations are shown in Figure 12.a. During iterations 1–10, the FFT plot, shown in Figure 12, highlights the magnitude of the target frequency growing dominant as other frequencies diminish. By the tenth iteration, only the target frequency remains significant. In the initial iteration, the algorithm identifies a relatively high motor step interval value among the five candidates. However, as iterations progress, the optimal motor step interval steadily converges toward the target value, as shown in Figure 12.c, and the fitness function consistently improves, confirming the algorithm's effectiveness (Figure 12.d). To prevent resonance and potential structural damage, the optimization is halted once the objective is successfully met.

Fig. 11. Sensor placement at point J, center of the third-story beam

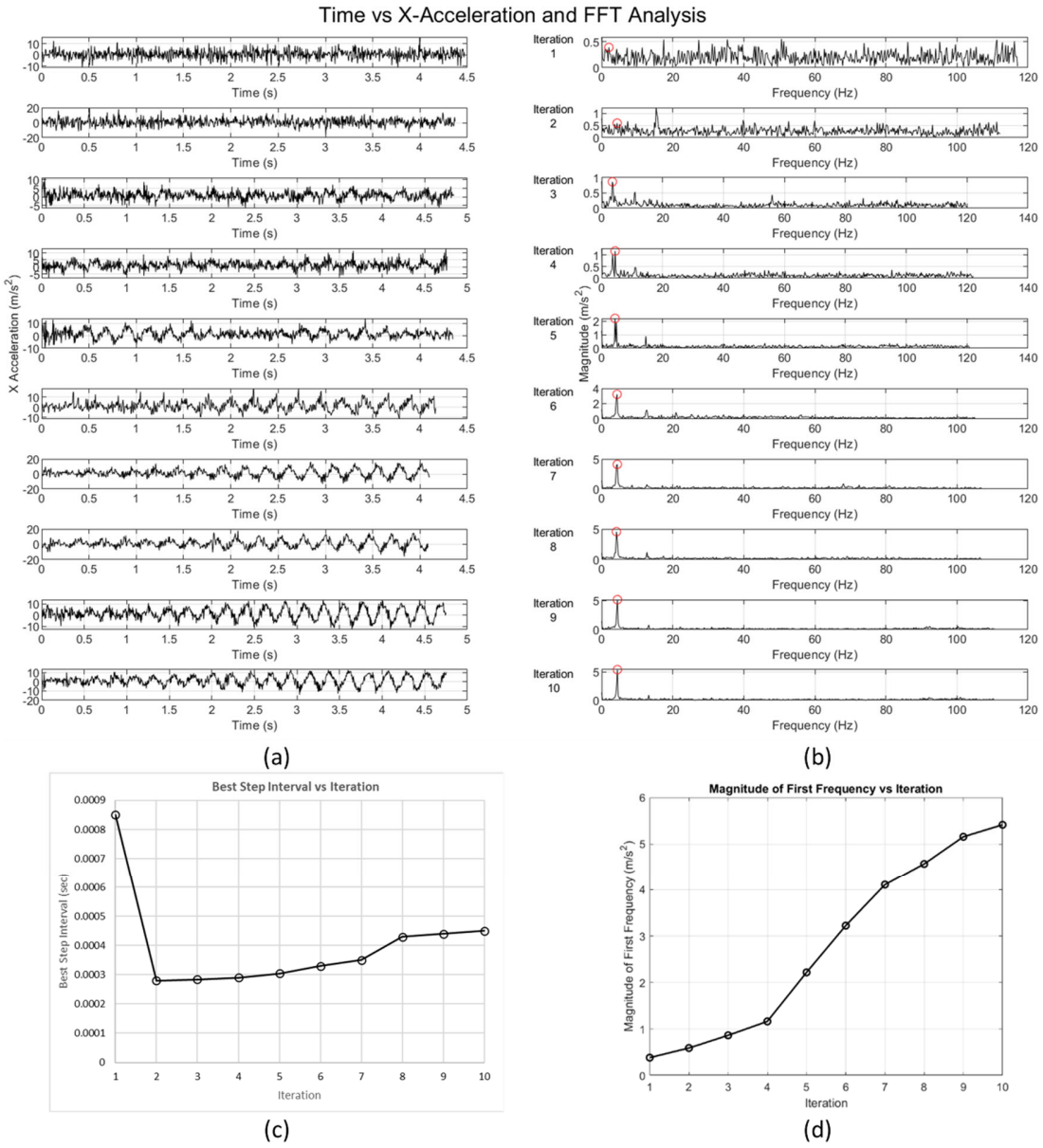

Fig. 12. Algorithm results at point J – (a) X-axis acceleration for best particle per iteration, (b) Acceleration FFT, (c) Best motor step interval vs. iteration, (d) Fitness values vs. iteration

5.4. Sensor placement at point J

The sensor is positioned at 1000 mm in the middle of the second-story beam (Point M, Figures 5a and 10). Figure 14.a illustrates the recorded accelerations for the best particle at each iteration. During iterations 1–10, the FFT plot shown in Figure 14b indicates that the magnitude of the target frequency becomes increasingly dominant as other frequencies diminish. By the tenth iteration, the target frequency remains the only significant component. Figure 14.c, the motor step interval progressively aligns with the target value as the number of iterations increases while the fitness function improves, validating the algorithm's performance (Figure 14d). To avoid inducing resonance and potential structural damage, the optimization process is terminated once the objective is achieved.

Fig. 13. Sensor placement at point M, center of the second-story beam

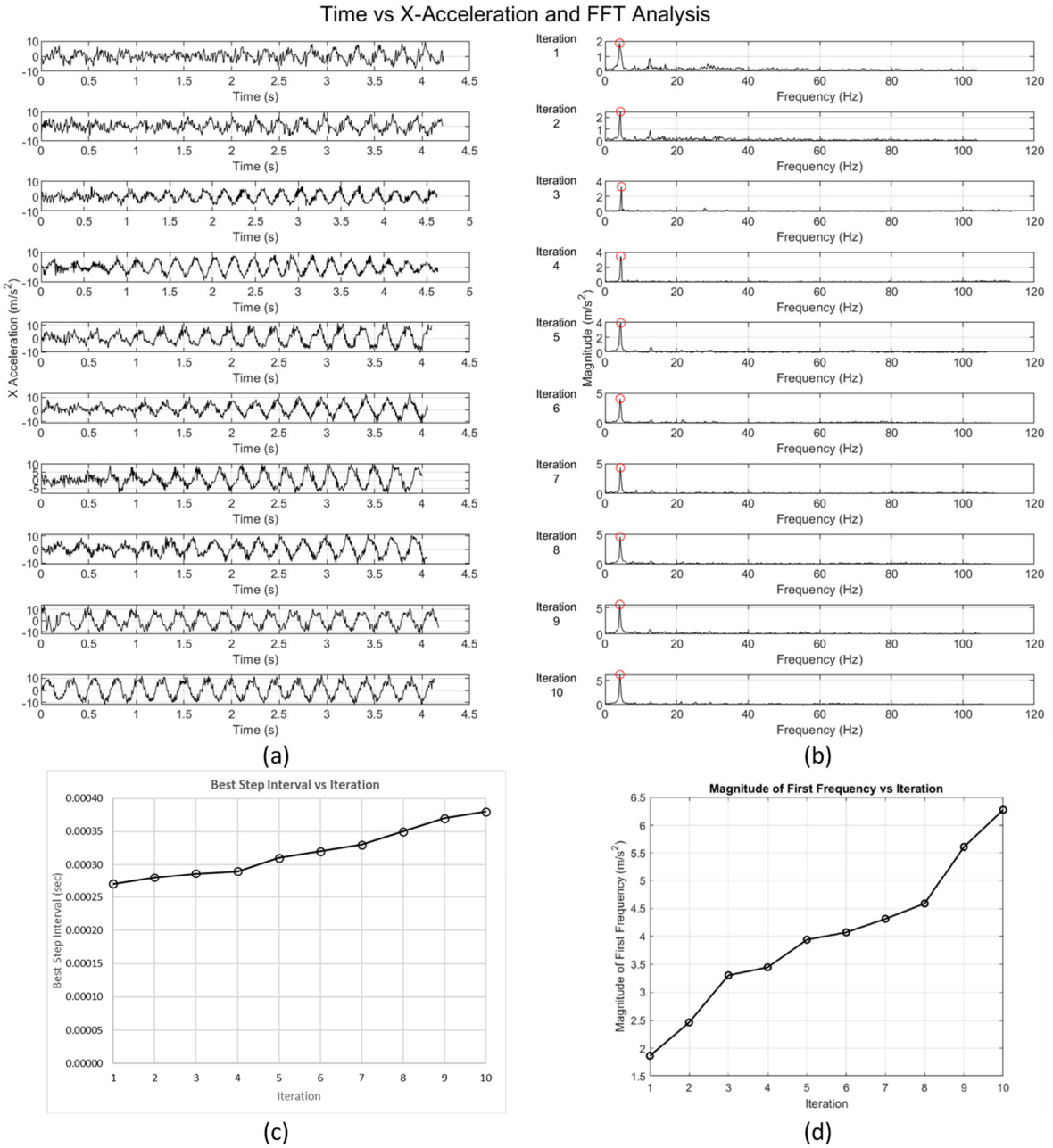

Fig. 14. Algorithm results at point M – (a) X-axis acceleration for best particle per iteration, (b) Acceleration FFT, (c) Best motor step interval vs. iteration, (d) Fitness values vs. iteration

6. Results

The results of this study highlight the effectiveness of the proposed system in achieving resonance within structural components through a combination of precise hardware design and algorithmic optimization. The PSO algorithm successfully tuned the motor step interval to amplify the target frequency, as evidenced by the steadily increasing magnitude of the target mode in the FFT plots. By the tenth iteration, the target frequency was the sole prominent component, demonstrating the system's ability to isolate and enhance the desired mode. This optimization process was adaptive, converging efficiently despite no prior knowledge of the structure's dynamic properties.

The system's robustness is further demonstrated by its consistent performance across different sensor placements. At Point P, the acceleration magnitude increased by 2084% (from 0.132 m/s² to 2.751 m/s²). Similarly, Points M and L exhibited amplification gains of 1392% and 1092%, with final accelerations of 5.413 m/s² and 5.623 m/s², respectively. Point J displayed the smallest increase (336%, from 1.866 m/s² to 6.276 m/s²), which can be attributed to the relationship between sensor elevation and resonance values. Table 2 summarizes these results, showcasing the variation in performance based on sensor placement.

Table 2: Device Specifications

Sensor Point	Initial Acceleration (m/s²)	Final Acceleration (m/s²)	FFT Gain (%)
P	0.132	2.751	2084 %
M	0.389	5.413	1392 %
L	0.515	5.623	1092 %
J	1.866	6.276	336 %

The results showcase three key features of the system's performance. First, significant acceleration increases were observed across all sensor locations, with the largest gains recorded at Point P, demonstrating the system's ability to generate substantial vibrational forces. Second, signal amplification was achieved through the optimization of the motor step interval by the PSO algorithm, effectively aligning the mass's motion with the structure's natural frequency to enhance resonance. Lastly, the system displayed adaptability to the structure's dynamic characteristics, consistently refining the step interval over iterations to maximize resonance and achieve precise tuning without prior knowledge of the structural properties.

These findings highlight the potential of the proposed system for applications in SHM, non-destructive testing, and vibration analysis. The device's ability to uncover modal information from structural points that typically contribute little to ordinary data acquisition is particularly promising. This capability provides more comprehensive insights into structural behavior, enabling the precise formulation of objective functions and the identification of dynamic characteristics. The results also suggest future enhancements, such as incorporating dynamic termination criteria, that could further improve system performance while maintaining structural

safety. The results underscore the adaptability and efficacy of the system in resonance optimization, paving the way for advanced autonomous solutions in structural analysis.

Conclusion

This study successfully developed and validated a device for inducing and optimizing structural resonance using a stepper motor, an ADXL345 accelerometer, and a PSO algorithm. The system demonstrated its ability to adaptively tune the motor speed by adjusting the step interval to resonate with the target frequency, significantly amplifying structural vibrations. Key findings include the algorithm's consistent convergence towards the optimal motor speed, the suppression of undesired frequencies, and the steady improvement in fitness function values across iterations. The experiments confirmed the device's adaptability and effectiveness in optimizing resonance, even without detailed prior knowledge of the structure. The system's design also prioritizes structural safety by imposing iteration limits to prevent excessive resonance and potential damage. This balance of optimization and safety makes the device highly suitable for applications in SHM, non-destructive testing, and active vibration control. Future research will focus on enhancing the device's capabilities, including dynamic termination criteria, expanded testing under varied conditions, and integration with more complex structures. The findings of this study contribute to the advancement of autonomous resonance-based monitoring systems, supporting the development of safer and more resilient infrastructure.

Acknowledgment

This work was supported by Shahid Rajaee Teacher Training University under grant number 9406.

References

[1] A. Sabato, C. Niezrecki, G. Fortino, Wireless MEMS-based accelerometer sensor boards for structural vibration monitoring: A review, IEEE Sensors Journal, Vol. 17, Iss. 2, 226-235 (2016).

[2] P. Ragam, N. Devidas Sahebraoji, Application of MEMS-based accelerometer wireless sensor systems for monitoring of blast-induced ground vibration and structural health: a review, IET Wireless Sensor Systems, Vol. 9, Iss. 3, 103-109 (2019).

[3] H. Baghdadi, K. Rhofir, M. Lamhamdi, Smart portable system for monitoring vibration based on the Raspberry Pi microcomputer and the MEMS accelerometer, Int J Inf & Commun Technol, Vol. 12, Iss. 3, 261-271 (2023).

[4] M. Marinaki, Y. Marinakis, G.E. Stavroulakis, Vibration control of beams with piezoelectric sensors and actuators using particle swarm optimization, Expert Systems with Applications, Vol. 38, Iss. 6, 6872-6883 (2011).

[5] M.U. Saeed, Z. Sun, S. Elias, Research developments in adaptive intelligent vibration control of smart civil structures, Journal of Low Frequency Noise, Vibration and Active Control, Vol. 41, Iss. 1, 292-329 (2022).

[6] L. Huang, Q. Li, Y. Qin, X. Ding, M. Zhang, L. Zhao, Structural design and optimization of a resonant micro-accelerometer based on electrostatic stiffness by an improved differential evolution algorithm, Micromachines, Vol. 13, Iss. 1, 38 (2021).

[7] M. Brunelli, A. Fusi, F. Grasso, F. Pasteur, A. Ussi, Torsional vibration analysis of reciprocating compressor trains driven by induction motors, IOP Conference Series: Materials Science and Engineering, IOP Publishing, 2015, pp. 012021.

[8] S.S. Saidin, A. Jamadin, S. Abdul Kudus, N. Mohd Amin, M.A. Anuar, An overview: The application of vibration-based techniques in bridge structural health monitoring, International Journal of Concrete Structures and Materials, Vol. 16, Iss. 1, 69 (2022).

[9] T.E. Saaed, G. Nikolakopoulos, J.-E. Jonasson, H. Hedlund, A state-of-the-art review of structural control systems, Journal of Vibration and Control, Vol. 21, Iss. 5, 919-937 (2015).

[10] F. Al-Badour, M. Sunar, L. Cheded, Vibration analysis of rotating machinery using time–frequency analysis and wavelet techniques, Mechanical Systems and Signal Processing, Vol. 25, Iss. 6, 2083-2101 (2011).

[11] T. Wang, J. Song, Harmonic Detection Method Based on Particle Swarm Optimization and Simulated Annealing Algorithm of Electrohydraulic Servo System, Journal of Robotics, Vol. 2022, Iss. 1, 7483427 (2022).

[12] J. Yao, H. Yu, M. Dietz, R. Xiao, S. Chen, T. Wang, Q. Niu, Acceleration harmonic estimation for a hydraulic shaking table by using particle swarm optimization, Transactions of the Institute of Measurement and Control, Vol. 39, Iss. 5, 738-747 (2017).

[13] V. Gupta, M. Sharma, N. Thakur, Optimization criteria for optimal placement of piezoelectric sensors and actuators on a smart structure: a technical review, Journal of Intelligent Material Systems and Structures, Vol. 21, Iss. 12, 1227-1243 (2010).

[14] I. Bruant, L. Proslier, Improved active control of a functionally graded material beam with piezoelectric patches, Journal of Vibration and Control, Vol. 21, Iss. 10, 2059-2080 (2015).

[15] I. Bruant, L. Proslier, Optimal location of piezoelectric actuators for active vibration control of thin axially functionally graded beams, International Journal of Mechanics and Materials in Design, Vol. 12, 173-192 (2016).

[16] M. Biglar, H.R. Mirdamadi, Configuration optimization of piezoelectric patches attached to functionally graded shear-deformable cylindrical shells considering spillover effects, Journal of Intelligent Material Systems and Structures, Vol. 27, Iss. 3, 295-313 (2016).

[17] D. Chhabra, G. Bhushan, P. Chandna, Optimal placement of piezoelectric actuators on plate structures for active vibration control via modified control matrix and singular value decomposition approach using modified heuristic genetic algorithm, Mechanics of advanced materials and structures, Vol. 23, Iss. 3, 272-280 (2016).

[18] M. Nezami, B. Gholami, Optimal locations of piezoelectric patches for supersonic flutter control of honeycomb sandwich panels, using the NSGA-II method, Smart Materials and Structures, Vol. 25, Iss. 3, 035043 (2016).

[19] K. Bendine, F. Boukhoulda, B. Haddag, M. Nouari, Active vibration control of composite plate with optimal placement of piezoelectric patches, Mechanics of Advanced Materials and Structures, Vol. 26, Iss. 4, 341-349 (2019).

[20] J.J. Moghaddam, A. Bagheri, A novel stable deviation quantum-behaved particle swarm optimization to optimal piezoelectric actuator and sensor location for active vibration control, Proceedings of the Institution of Mechanical Engineers, Part I: Journal of Systems and Control Engineering, Vol. 229, Iss. 6, 485-494 (2015).

[21] E. Lu, W. Li, X. Yang, Y. Wang, Y. Liu, Optimal placement and active vibration control for piezoelectric smart flexible manipulators using modal H 2 norm, Journal of Intelligent Material Systems and Structures, Vol. 29, Iss. 11, 2333-2343 (2018).

[22] J. Kennedy, R. Eberhart, Particle swarm optimization (PSO), Proc. IEEE International Conference on Neural Networks, Perth, Australia, 1995, pp. 1942-1948.

[23] D. Wang, D. Tan, L. Liu, Particle swarm optimization algorithm: an overview, Soft computing, Vol. 22, Iss. 2, 387-408 (2018).

[24] M. Worth, A. Gaul, S. Jager, P. Omenzetter, H. Morris, Dynamic performance assessment of a multistorey timber building via ambient and forced vibration testing, continuous seismic monitoring and finite element model updating, World Conference on Timber Engineering, 2012.

[25] Á. Cunha, E. Caetano, Experimental modal analysis of civil engineering structures, (2006).

[26] C. Krämer, C. De Smet, B. Peeters, Comparison of ambient and forced vibration testing of civil engineering structures, Proceedings of IMAC, 1999, pp. 1030-1034.

[27] F. Shabbir, P. Omenzetter, Forced vibration testing of a thirteen storey concrete building, 2008 NZSEE Conference, Taupo, New Zealand, 2008.

[28] A. Havaran, M. Mahmoudi, Extracting structural dynamic properties utilizing close photogrammetry method, Measurement, Vol. 150, 107092 (2020).

[29] A.Z.B. Nejad, M.M. Sahebi, An investigation on the capability of proper orthogonal modes in determining the natural frequencies and damping ratios of linear structural systems, Engineering Structures, Vol. 243, 112691 (2021).